PNAS

Supporting Information for

Predicting resilience of migratory birds to environmental change

Simeon Lisovski (0000-0002-6399-0035)[1], Bethany J. Hoye (0000-0001-9502-5582)[2], Jesse R. Conklin (0000-0002-1414-0587)[3], Phil F. Battley (0000-0002-8590-8098)[4], Richard A. Fuller (0000-0001-9468-9678)[5], Ken B. Gosbell[6], Marcel Klaassen (0000-0003-3907-9599)[6,7], Chengfa Benjamin Lee (0000-0002-2207-5615)[8], Nicholas J. Murray (0000-0002-4008-3053)[9], Silke Bauer (0000-0002-0844-164X)[10,11,12]

[1] Alfred Wegener Institute Helmholtz Centre for Polar and Marine Research, Polar Terrestrial Systems, 14473 Potsdam, Germany. [2] School of Earth, Atmospheric and Life Sciences, University of Wollongong, Wollongong, NSW, Australia. [3] Conservation Ecology Group, Groningen Institute for Evolutionary Life Sciences (GELIFES), University of Groningen, Groningen, The Netherlands. [4] Zoology and Ecology Group, Massey University, Palmerston North, New Zealand. [5] University of Queensland, Brisbane, Australia. [6] Victorian Wader Study Group, Melbourne, Australia. [7] Centre for Integrative Ecology, School of Life and Environmental Sciences, Deakin University, Waurn Ponds Campus, Victoria 3217, Australia. [8] German Aerospace Center (DLR), Remote Sensing Technology Institute (IMF), Rutherfordstr. 2, 12489 Berlin, Germany. [9] College of Science and Engineering, James Cook University, Townsville, Queensland, Australia. [10] Department of Bird Migration, Swiss Ornithological Institute, Sempach, Switzerland. [11] Institute of Biodiversity and Ecosystem Dynamics, University of Amsterdam, The Netherlands, [12] Department of Environmental Systems Science, ETH Zürich, Switzerland

* Simeon Lisovski

Email: Simeon.Lisovski@gmail.com

This PDF file includes:

- S1: Model description
- S2: Environmental parameters
- S3: Species parameters
- SI References

Code availability:

Lisovski, S. Model code: Predicting resilience of migratory birds to environmental change. GitHub release v0.1. Zenodo. DOI:10.5281/zenodo.10396366

S1: Model description

State-dependent optimality models calculate fitness-maximizing decisions depending on time and a set of state-variables – in our case, location and body reserves. They use an optimization procedure (linear programming) that starts at the final time-point and calculate backwards the sequence of behavioural decision that would maximize fitness. Fitness differences are defined in reproductive output, i.e. the number of fledglings per adult bird in the respective year.

The fundamental behavioural decisions for each time-step in the model are to either stay at its present location or migrate to one of the following sites. Each decision has consequences for the animal's state (body reserves and location): Staying at the present location may allow foraging and accumulating fuel stores that are required for covering the next migratory step or for accumulating reserves required for breeding. However, staying and foraging also entails mortality risks – as carrying body reserves may be costly (1) and foraging may reduce vigilance (see below), and a time-cost when staying beyond the best time for arrival at the breeding grounds. Alternatively, flying to one of the following sites may bring a bird closer to its breeding grounds and thus, facilitate arrival at the breeding grounds within the short time-window that allows successful breeding. However, if this 'target-site' does not provide food yet, staying there might increase starvation risk.

Once the optimal decisions have been calculated for all possible combinations of time, body reserve levels and for all locations, forward simulations are run to generate predictions on individual birds during their journey from the wintering to breeding grounds.

State variables

Birds were characterized by their body reserves, x, which may vary between 0, when the bird has reached a minimum body mass, has no reserves and is assumed to die of starvation, and x_{max} = 100 where the bird has reached its maximum fuel load. For example, minimum and maximum body mass of a Red Knot (*Calidris canutus*), are 110 and 210 g, and given an energy content of fuel of 32.77 kJ/g (2), x_{max} corresponds to 3277 kJ. Body reserves may increase with foraging and decrease during migratory flights (see below). The migration period was divided into whole days, t, starting 1 January onwards.

The terminal reward is a central part of the model and specifies the fitness-consequences of arrival in the breeding grounds (and thus, the starting point of the backward calculations). In migratory birds, which breed in Northern or Arctic breeding grounds, both arrival time and body condition at arrival determine their expected reproductive success for the present year. In addition, if birds arrive too late or in low body condition, they cannot successfully breed this year but may attempt breeding in future years. Based on empirical studies (e.g., 3), we know that migratory shorebirds might not be capital breeders, i.e. their reproductive output is weakly linked to the level of body reserves brought to the breeding grounds.
We use the following relation between state at arrival and number of young produced:

$$R(x) = \frac{1}{2}\left(\frac{\exp(w(x - x_c)) - \exp(-w(x - x_c))}{\exp(w(x - x_c)) + \exp(-w(x - x_c))} + 1 \right), \qquad \text{eqn A1}$$

where w= 0.028 and x_c = 10.

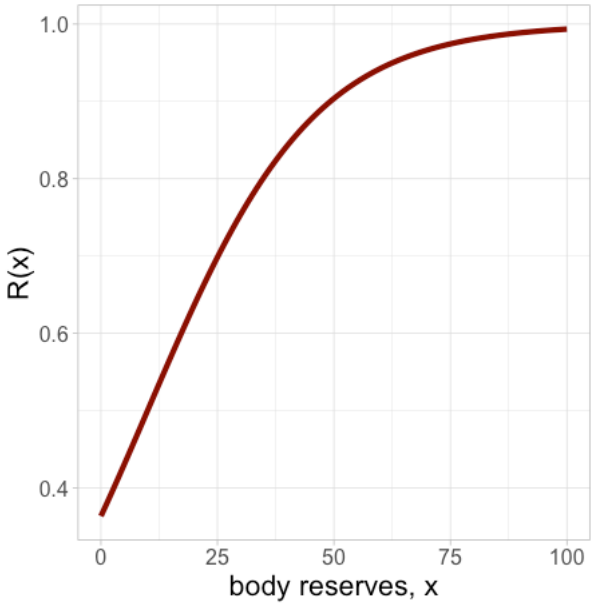

Figure S 1: Body condition at arrival in the breeding grounds influences reproductive investment, i.e., the number of young expected from this year's breeding attempt increases quickly with the level of body reserves ('income breeding').

In most Arctic breeding birds, successful breeding is only possible if birds arrive within a rather narrow time-window on their breeding grounds. Arriving outside this period leads to breeding failure either because birds arrive too late to raise offspring able to survive or too early jeopardizing their own fitness (4).

$$K(t) = \begin{cases} 0 & if\ t < t_{\min}\ or\ t > t_{\max} \\ 1 & if\ t_{\min} \le t \le t_{\max} \end{cases}$$ eqn A2

The time window was set using the date of snowmelt on the breeding site (see S2: Environmental parameters). When arriving at the breeding grounds outside this period a fitness gain can thus only be achieved from future breeding attempts, *B*, which depends on survival and reproductive success in future breeding attempts. As detailed data are usually lacking on how current body reserves influence future reproduction or survival in a species, we tentatively set *B* = 3, reflecting a relatively long-lived species. Although it may seem that adding this constant future reproductive success is unnecessary, it can drive trade-offs between the current and future reproduction. Perhaps more important even, it separates fatal from unsuccessful strategies, i.e., strategies that would lead to, e.g., death by starvation, and strategies that only loose current reproductive outcome, e.g., by arriving too late or with very little body stores. A bird's overall fitness is thus determined by

$$F(x,t,N) = K(t) \cdot R(x) + B$$ eqn A3

In each time-step, a bird may choose to remain on its present location or to migrate to another site. If remaining on the present site, a bird requires energy, *e*, for maintaining its metabolism (see also S3: Species parameters). When staying, a bird may choose to forage with intensity *u*. If gain from foraging exceeds expenditure, the bird's energy reserves increase, while they are depleted when foraging gains are lower than expenditure. Since there might be stochastic differences in individual foraging success, we modelled the gain rate as a discrete random variable with outcomes $g_1(i), \ldots g_j(i), \ldots, g_{max}(i)$ and the probability of achieving a particular maximum gain is given by

$$P\left[G = g_j(i)\right] = p_j(i), \text{ where } \sum_j p_j(i) = 1$$ eqn A4

Stochastic differences in foraging success imply that there might be series of 'bad luck' in foraging, during which an animal could starve to death when reserves are insufficient.

Accounting for this will often yield a foraging intensity that is different from a foraging intensity that results from deterministic foraging success.

The maximum gain can differ between sites. The foraging intensity *u* (0 <= *u* <= 1) is the fraction of the maximum gain *G* that birds will deposit given the maximum body reserves level is not exceeded. Consequently, if a bird with body reserves *x* forages with intensity *u* at site *i*, its body reserves in the next time-step will be $x + ug_j(i) - e$.

Maintaining fuel stores and foraging incurs fitness costs in terms of increased risk of predation or injury (1). We assume the daily 'predation' risk *m(x,u,i)* depends on foraging intensity (as this reduces vigilance) and carrying body stores (as this reduces manoeuvrability and/or escape behaviour) and define it as follows (5):

$$m(x,u,i) = m_0(i) + b_1(i)\frac{(x+ug_j(i))^{a_1+1} - x^{a_1+1}}{(a_1+1)ug_j(i)} \cdot b_2(i)u^{a_2} \qquad \text{eqn A5}$$

with background predation risk, $m_0 = 10^{-3}$, mass-dependent coefficient $b_1 = 10^{-4}$, foraging-intensity-dependent coefficient $b_2 = 10^{-6}$ and a_1 and a_2 the mass- and foraging-dependent exponents, which were set to 2, foraging intensity, *u*, (0 <= *u* <=1) and stochastic gain $g_j(i)$ at site *i* (see eqn A4 above). Although the coefficients are chosen such that the predation risk *m(x, u, i)* is typically much smaller than one, we constrain 0 <= *m(x,u,i)* <= 1 and for $u = 0.0$, we set $m(x,u,i) = m_0(i)$.

Please note that with this approach, predation risk is not fixed per se but, rather, is used to specify the *costs of behaviours* and the *costs of being in a specific state* (Fig. S2). Animals can respond to these costs by adjusting their behaviour such that they minimize mortality, or rather, maximize fitness and an optimization procedure evaluates these costs and benefits for the animal's current state and identifies the trade-off (the best *u*) between avoiding starvation and predation, and gaining energy.

If the bird decides to forage, it should forage with an intensity *u* that yields the maximum expected fitness:

$$H_f(x,t,i) = \max_u[(1-m(x,u,i))F(x+ug(i,t)-e,t+1,i)] \qquad \text{eqn A6}$$

Alternatively, a bird may decide to migrate to a following or a preceding site given its body reserves permit to cover the distance *D* to the destination site. Consequently, its body reserves upon arrival, x_a, at this destination are (6):

$$x_a = \left(\frac{c^2}{c - \left(c\left(1 - \left(1 + x/x_{\max}\right)^{-0.5}\right) - D \right)^2} - 1 \right) \cdot x_{\max} \qquad \text{eqn A7}$$

where *c* is a flight range parameter which is calculated using

$$c = \frac{D_{\max}}{1 - \left(1 + x_f / x_{\max}\right)^{-0.5}} \qquad \text{eqn A8}$$

and D_{max} is the maximum flight range when dedicating fraction x_f of the maximum fuel load x_{max} to flight. In this study we used $x_f = x_{max}$. D_{max} was calculated by dividing the maximum fuel load by the flight costs in terms of energy over time:

$$D_{\max} = \frac{x_{\max}}{f} \qquad \text{eqn A9}$$

Species specific parameters can be found in S3: Species parameters.

If an individual decides to depart, it should fly to the site *j* yielding the maximum expected fitness at the destination:

$$H_d(x,t,i) = \max_j [F(x_a, t + (\sum_{z=i}^{j-1} D_z / v), j)] \qquad \text{eqn A10}$$

where *v* is flight speed.

The optimal decision is the behavioural alternative, foraging or departing, yielding the highest future expected reproductive success:

$$F(x,t,i) = \max[H_f(x,t,i), H_d(x,t,i)] \qquad \text{eqn A11}$$

With the dynamic programming equations, a matrix can be compiled containing the optimal behavioural decisions for all combinations of fuel stores, times and sites. Furthermore, we used the errors in decision making approach, which allows deviations from perfectly optimal behaviour given such deviations have only little cost (7). Consequently, for each action a probability is calculated, with which this action is performed, and which depends on the fitness consequences of this action.

These probabilities are then used in subsequent forward simulations to follow individual birds during their journey and to generate predictions of individual migratory behaviour, i.e., departure and staging times and, more importantly, to quantify the fitness consequences of given environmental circumstances.

Forward simulation

Using the optimal decision matrix, we followed individual birds on their migration to the breeding grounds using a Monte-Carlo simulation method. To this end, and for each empirically tracked individual (individual start and end point), and for each scenario, we let a population of 100 individuals with random distributed initial body reserves of x between 30 and 50 start in the wintering site at t = 0. Thereafter, all individuals behave nearly optimally according to their present body reserves, site, and time by performing an action, i.e., migrating to site j or staying and foraging with intensity u, with probabilities corresponding to their fitness reward. The fuel gain at a given site is determined by a random number and the probability distribution of achieving the maximum gain (Eqn. A4).

From these individual migrations, departure times from the wintering site, staging times on any stop-over sites and arrival time in the breeding sites were recorded (See methods in main text).

S2: Environmental parameters

Flyway grid

The East Asian-Australasian Flyway was divided into a hexagonal grid (diameter of 400 km, and area of 138.564 km^2). All following calculations and data manipulations were applied on using an equal area projection ("+proj=laea +lat_0=15 +lon_0=162 +x_0=0 +y_0=0 +a=6370997 +b=6370997 +units=m +no_defs").

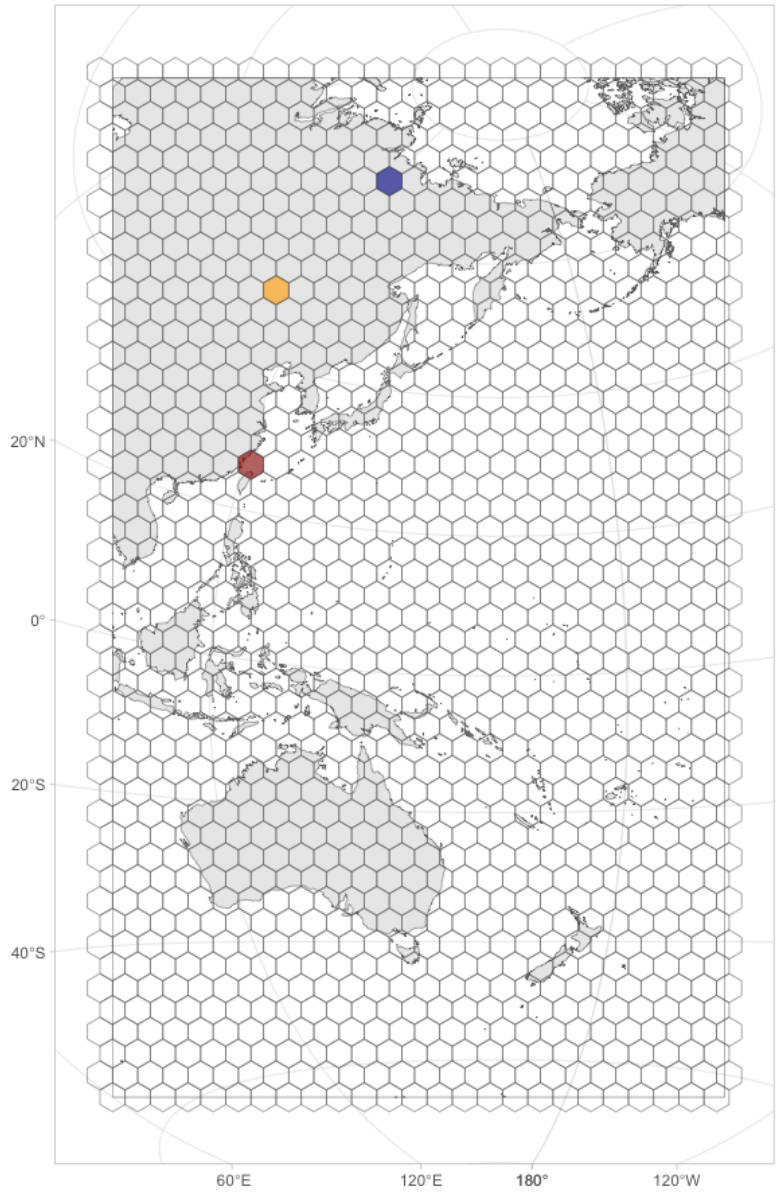

Figure S 2: Spatial hexagonal grid covering the East Asian-Australasian Flyway. The colored grid cells (orange = 355, red = 303, blue = 574) are used below as exemplars of the environmental data contained in each grid cell.

Temperature

Dataset	Variable	Spatial resolution	Temporal resolution	Reference
NOAA NWS NCEP: daily mean air temperature from the NCEP Reanalysis	air.sig995	2.5 x 2.5 °	Daily – used for the 1960s and 2010s scenarios	(8, 9)
CMIP6 climate projections: SSP1-2.6 (AWI-CM-1-1-MR (Germany))	Near-surface air temperature		Daily – used for the 2060s scenarios	(10)

NCEP-NCAR Reanalysis 1 daily surface temperature data on a 2.5 x 2.5 degree resolution was downloaded for the periods from 1950-1970 and 2000-2020 from the NOAA data repository (8). For the future scenario (2060s), we downloaded daily near-surface temperature predictions, 'middle of the road' SSP1-2.6 degree temperature increase scenario, from the CMIP6 climate projection (SSP1-2.6 scenario, AWI-CM-1-1-MR Model), which is available on a daily temporal and 25km spatial resolution (10). Data were extracted for each grid cell, and the median per day and the three time periods was used to describe the daily temperature across the migration period for past (1950-1970), present (2000-2020), and future (2060-2070) conditions.

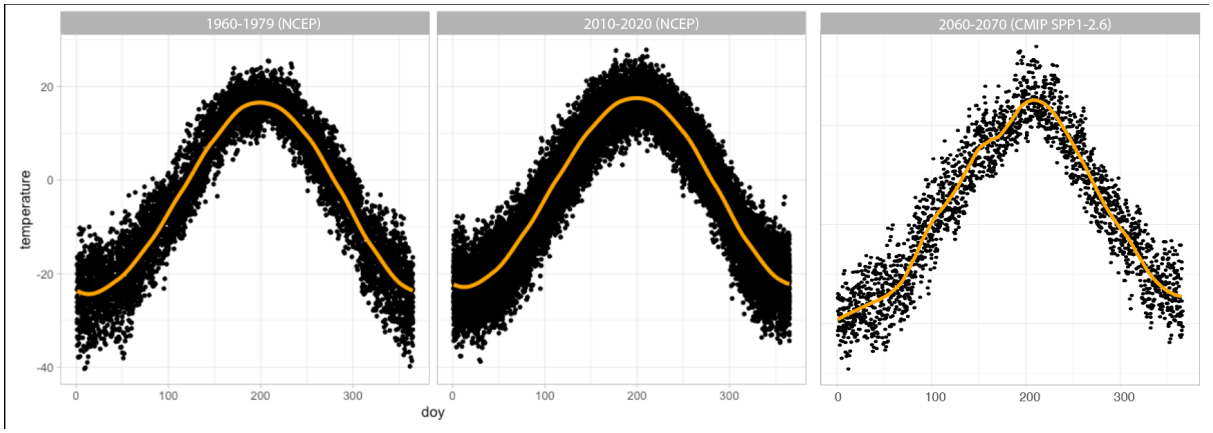

Figure S 3: Daily temperature (black dots) and median line (orange line) for a single grid id = 355 (orange cell in Figure S2) in all past, present and future scenarios.

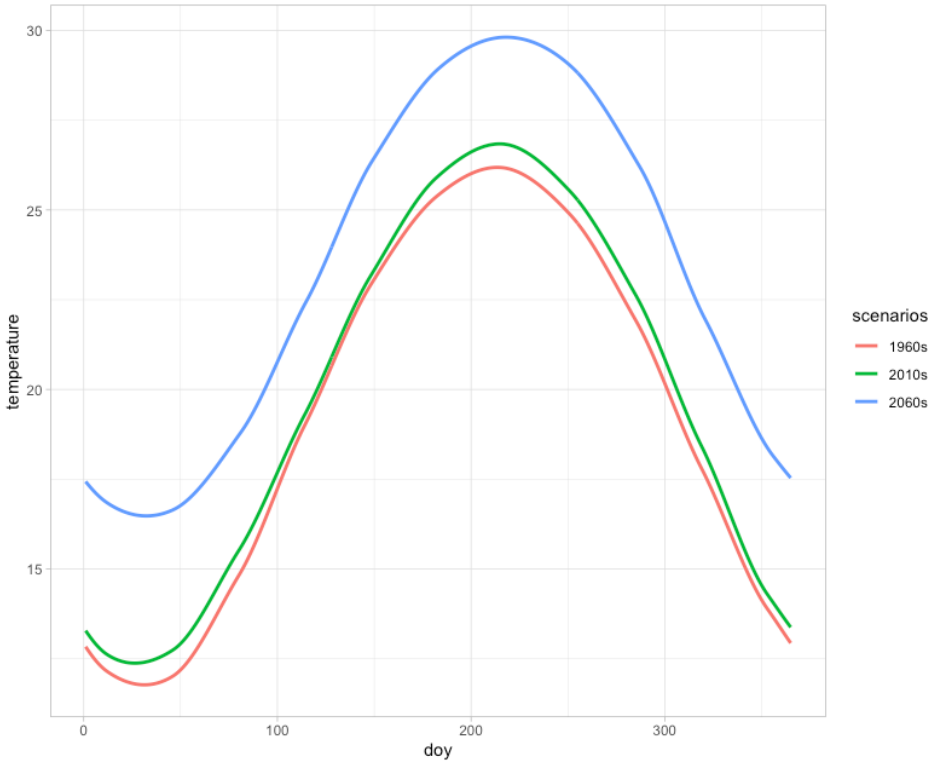

Figure S 4:Daily temperature for the three time periods and the single grid cell (id = 303)

Habitat maps (intertidal mudflats, mangroves)

Several datasets were used to define the quality of grid cells and thereby, their daily rates of energy intake and expenditure, that is ultimately linked with species specific fueling.

Dataset	Variable	Spatial resolution	Temporal resolution	Reference
Intertidal mudflats	extent	30 m	Annual	(11)
Historical intertidal mudflat extent in the Yellow Sea	extent	Spatial polygons	One time period (1950 – 1962)	(12)
Global Distribution of Mangroves USGS v1.3	Extent	2 km	One time period (1997-2000)	(13)
Natural Earth Data	Lakes	10 m	Present time	@naturalearthdata.com

First, the present extent of intertidal mudflats on a 30 x 30 m resolution were processed and downloaded via Google Earth Engine using the dataset described in (11). To avoid cutting mudflat areas by the border of the defined grid-cells (and underestimating the true extent of the mudflats), the extended area around each grid cell (400 km radius from the centre of each grid cell) was taken to define the km^2 of mudflats for each grid cell (Figure S 5). A historic dataset on the intertidal mudflat extent for the Yellow Sea Region and the entire Chinese coastline was used to define the past (1960s) habitat availability for all cells represented in this dataset (12). No change in intertidal mudflat extent was assumed for all other cells. In addition to intertidal mudflats, a third of the area of mangrove forests (not part of the Murray et al. 2019 dataset) growing in intertidal areas that partly provide resting and fueling habitat for migrating shorebirds, was added to the mudflat extent of each grid cell. The Global Distribution of Mangroves USGS v1.3 in km^2 units was downloaded from the UNEP-WCMC repository (13). Given the lack of data, no change in mangrove extent was included but extent was set constant over the time periods. Lakes in Australia, China and

Russia are known to provide important fueling and staging sites for migratory shorebirds during migration.

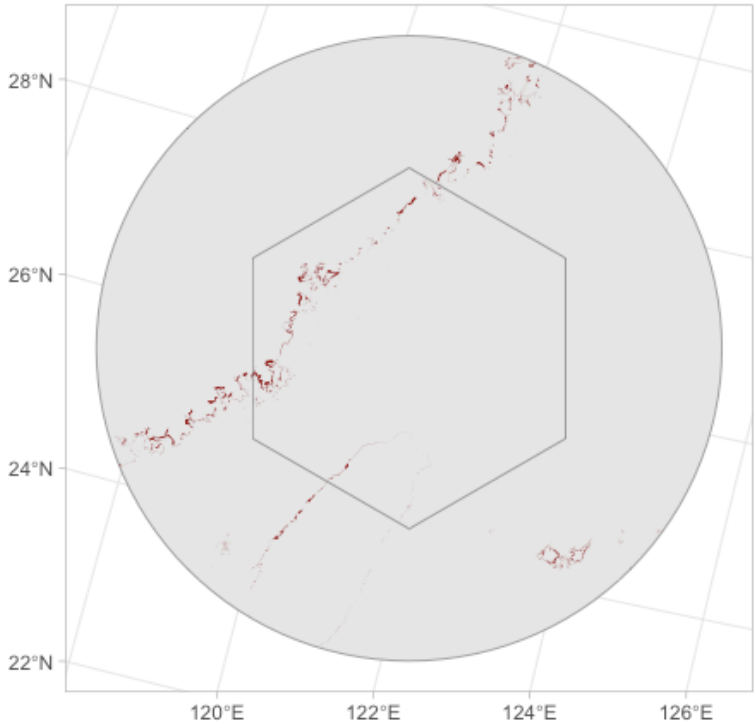

Figure S 5: Intertidal mudflats (red) in grid cell 303 and within the 400 km buffer zone.

Each cell without any mangrove or intertidal mudflat extent but with overlap of a lake larger than 1,500 km2 (n = 28, 90th percentile of lakes within the flyway, based in Natural Earth 10m Lake Dataset the free vector and raster map data @naturalearthdata.com) was flagged and removed for the model simulation. The extent of suitable habitat per grid cell was scaled between 0.5 and 1.5, indicating the relative value of a cell for foraging, and multiplied with the species-specific maximum energy intake rates (sites with lakes received a value of 1 for Red-necked Stint simulations, given their extensive use of inland lakes for fueling).

Snow melt timing

For each grid cell that lies in the estimated breeding site of individuals (as derived from the empirical tracks), the snowmelt timing for past (1960s) and present (2010s) condition was defined using the NOAA Northern Hemisphere Snow Cover Extent daily dataset (v01r01)

with an approx. 250 km spatial resolution (14). Snowmelt timing was calculated using a double sigmoidal fit for snow cover values (between 0 and 1) across the day of the year and applying a 0.75 threshold in spring, pooling data from 1950-1970 as well as 2010-2020.

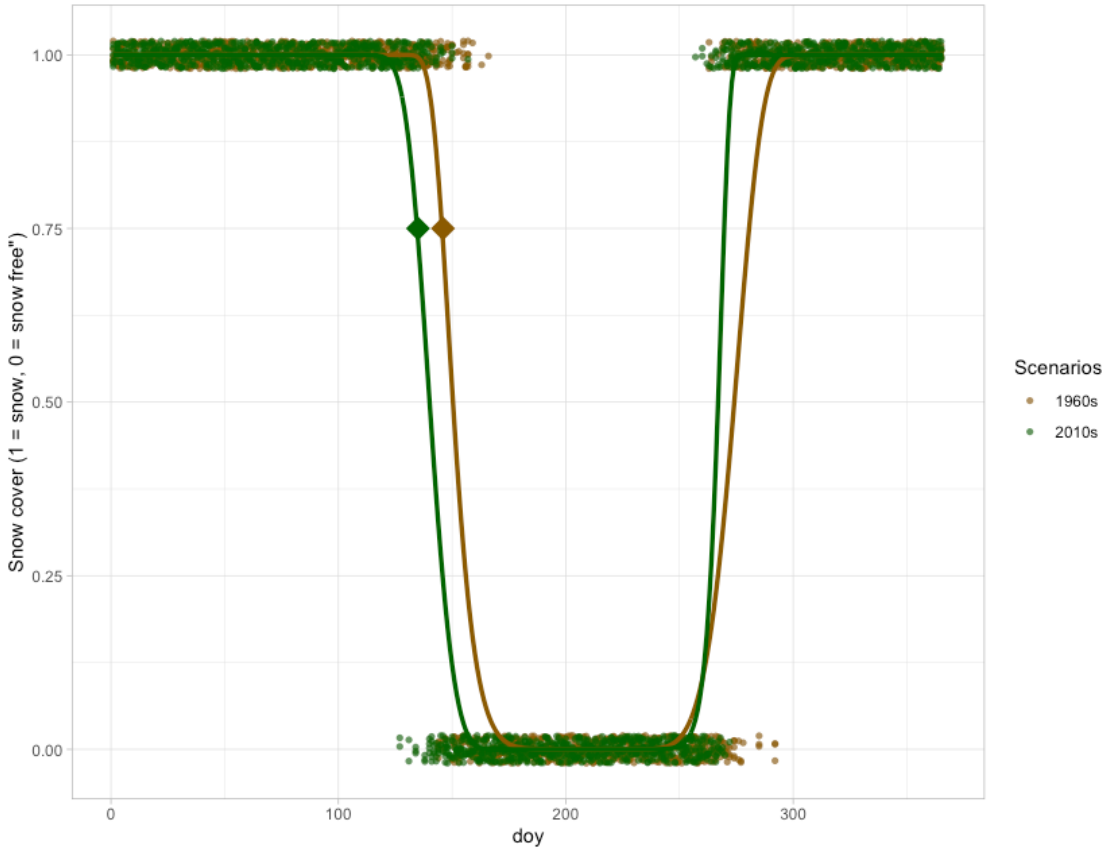

Figure S 6: Snow melt timing for the 1960s (brown) and the 2010s (green) based on sigmoidal model fit and a threshold of 0.75 (grid cell 574 from Figure S2).

Future (2060s) optimal arrival times were inferred from the relationship between snow melt date and temperature from the past (1960s) and current (2010s) conditions, given the lack of snow melt projections for the future, the snow melt date for the 2060s was determined by the relationship of temperature at the snowmelt day in the 1960s and 2010s.

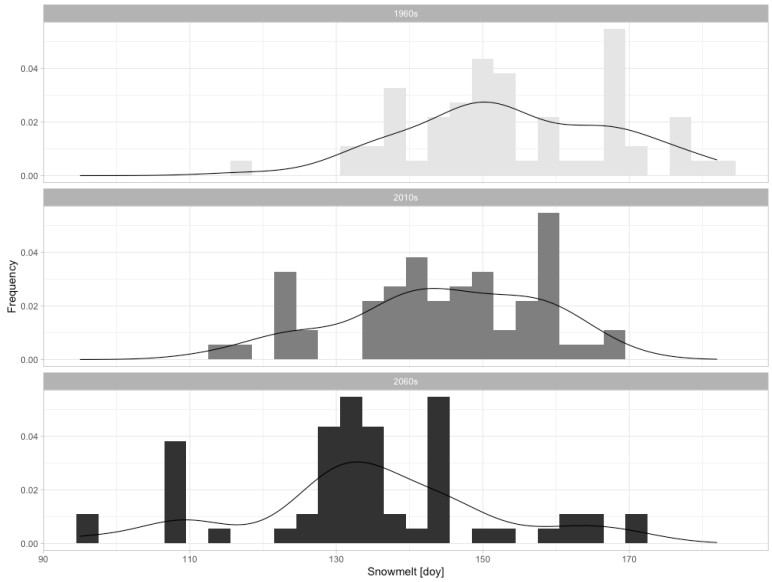

Figure S 7: Histograms of the timing of snowmelt for all breeding cells in the past (1960s), present (2010s) and projected future (2060s), based on temperature-snow melt relationship.

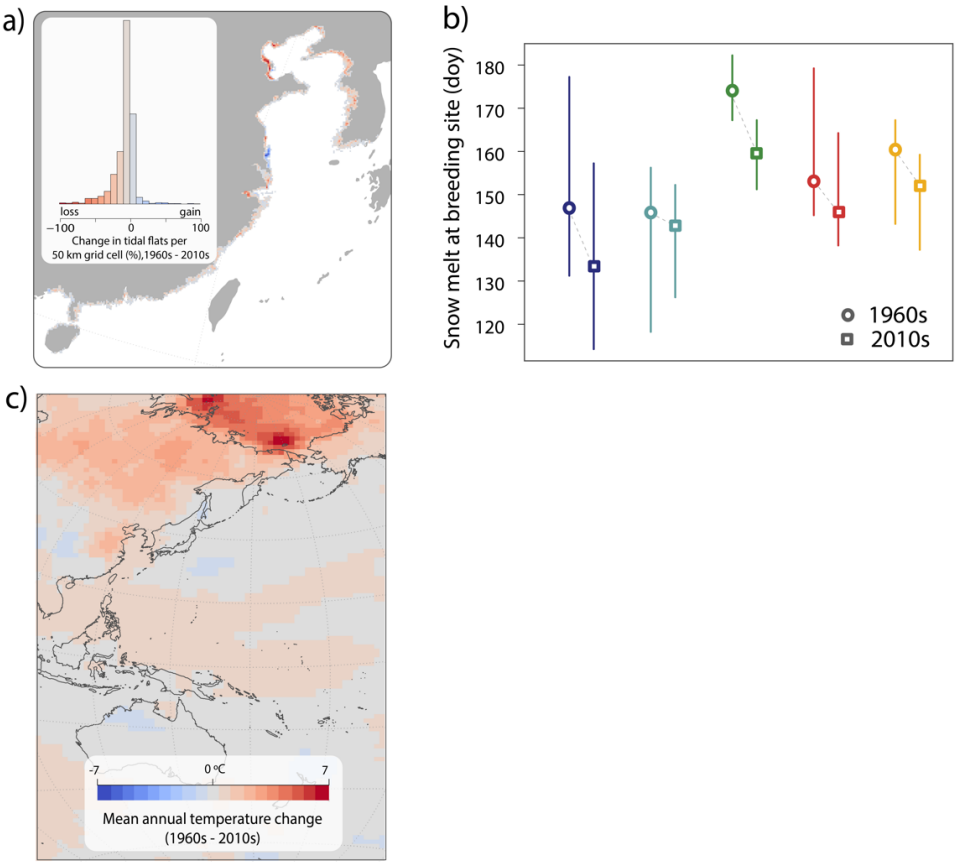

Figure S 8: Overall trends in environmental parameters across the flyway grid. a) shows changes in intertidal mudflat extent for areas with available historic data. b) shows changes in the spring snowmelt timing for all breeding sites of empirically tracked individuals (BTG, GN, RN, CS, RNS). c) shows mean annual temperature change across the flyway region.

S3: Species parameters

Some of the important parameters to define the physiological identity of the five different modelled shorebirds species were derived using established allometric relationships based on lean (BM_{min}) and maximum (BM_{max}) body mass (see Table S1).

Table S 1: Body mass (Lean and Maximum) derived from literature (15, 16). Relationship between body mass (g), x in the model and kJ used to calculate parameters.

Species	*BM_{min} [g]*	*BM_{max} [g]*	*g|x|kJ*
Bar-tailed Godwit	250	534	1|2.84|93.2
Great Knot	144	303	1|1.59|52.3
Red Knot	105	208	1|1.19|39.2
Curlew Sandpiper	55	110	1|0.49|16.1
Red-necked Stint	23	45	1|0.13|4.5

Fuel deposition rate

Based on maximum daily metabolizable energy intake (DME) and daily energy expenditure (DEE) for birds of different body mass, it is possible to estimate theoretical maximum fuel deposition rates (FDR_{max}), in relation to body mass. The fuel deposition rate for a given bird is the daily gain in fat mass as a percentage of lean body mass. The FDR_{max} for birds of different body masses (17) can be estimated as follows:

$$FDR_{max} = \frac{(DME_{max} - DEE_{min})}{M} \times \frac{\eta \times 100}{e} \qquad \text{eqn 12}$$

where (DME_{max} - DEE_{min}) gives the surplus energy in kJ per day that can be deposited, M is lean body mass in kg, η is the conversion efficiency of metabolising energy into fat, e is the energy value of the stored reserves in kJ kg^{-1} and 100 is for conversion into percentages.

Kirkwood (18) formulated DME_{max} as 173 x $M^{0.72}$ kj d^{-1}, where M is the body mass in kg and DEE_{min} is assumed to be 1.5 x BMR (basal metabolic rate).
For shorebirds, we used the relation of Lindstrom (17) 437 x $M^{0.73}$ kJ d^{-1}. Thus, the maximum fuel deposition rate will be:

$$FDR_{max} = 2.37 \times M^{-0.27} \quad \text{eqn 13}$$

Thus, the maximum rate at which fat can be deposited should decrease with increasing body mass, approximately in proportion to $M^{-0.27}$. However, when comparing the thus-obtained values with empirical data (see for details: summarized in Aharon-Rotman, Gosbell, Minton and Klaassen (19)), it shows that this relationships captures species differences well (Figure S 9) but slightly underestimates maximum fat deposition rates. This pattern likely results because empirical data were collected at different sites with different food quality, and likely also because shorebirds can forage for more hours a day than Kirkwood (18) allowed them in his experiments, see also (20), and indicates that the maximum fat deposition rates from eqn 13 are likely lower than the physiological maximum. Thus, in our modelling, we multiplied the maximum fat deposition rates of the sites with the largest intertidal mudflat extent with 1.5. By doing so, only 2% of the cells exceed the maximum fat deposition rates derived from the empirical dataset, a similar proportion (2.2%) of empirical measurements that exceeds the established fat deposition rate relationship with lean body mass (Figure S 9).

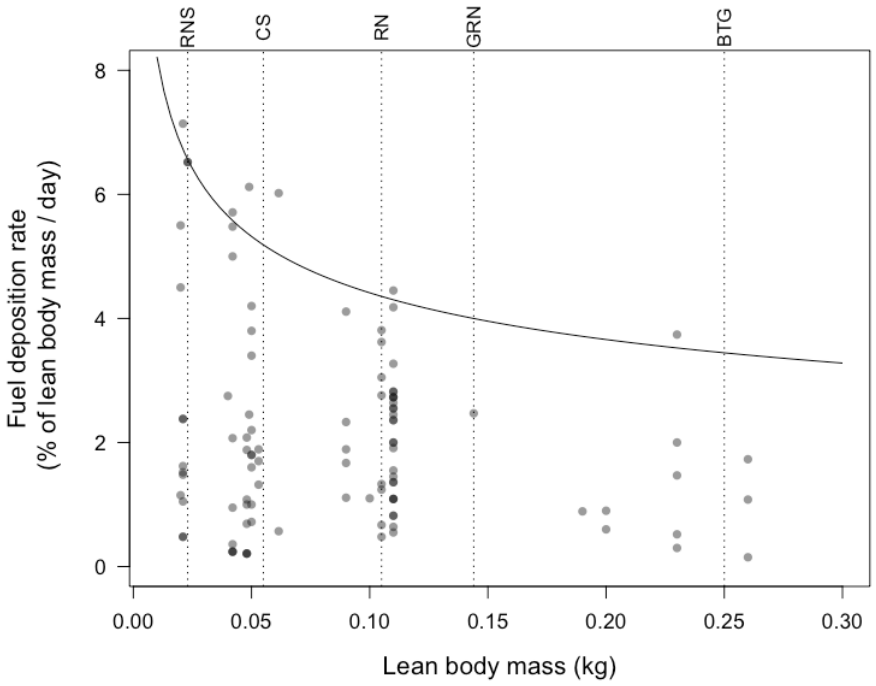

Figure S 9: Theoretical maximum fat deposition rate for shorebirds (solid line) as a function of body mass. Grey dots represent measured fat deposition rates in the field (extracted from Aharon-Rotman et al. (19)). Dashed lines show lean body mass for Red-necked Stints (RNS), Curlew Sandpiper (CS), Red Knot (RN), Great Knot (GRN) and Bar-tailed Godwit (BTG).

Energy expenditure

Animals always expend energy, even when they are inactive. Basal metabolic rate (BMR) is the energy expenditure of a non-productive, postabsorptive animal resting in thermoneutrality during the circadian rest phase (21). In our modelling framework, estimates of energy expenditure consist out of BMR plus the costs of thermoregulation.

BMR is body mass (BM) dependent and for shorebirds best described by the allometric relationship (22, Figure S 10):

$$BMR(Watts) = 5.06 \times BM(kg)^{0.729} \quad \text{eqn A14}$$

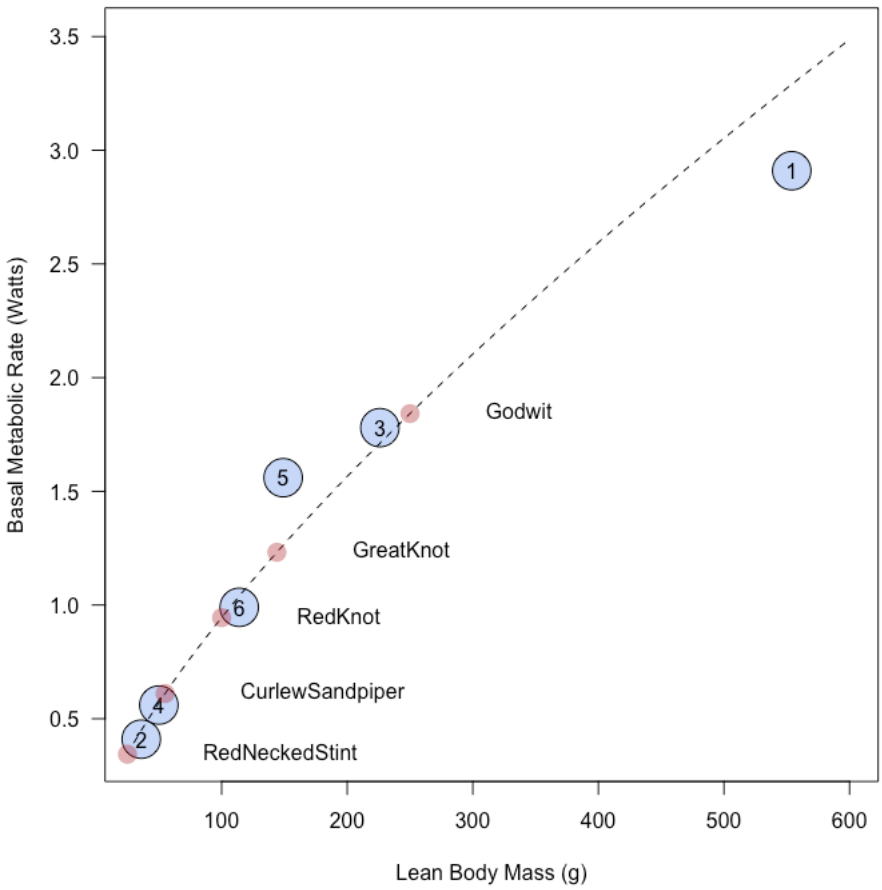

Figure S 10: Allometric relation between basal metabolic rate in relation to body mass after Kersten & Piersma (22). Predictions (dashed line) are based on correlation of measured basal metabolic rate at 10 degrees Celsius in six species (blue dots: 1. Oystercatcher, 2. Little Ringed Plover, 3. Grey plover, 4. Sanderling, 5. Redshank, 6. Turnstone). Red dots are predicted BMR values for the five species of this study.

Below thermoneutrality, metabolic rate increases linearly with decreasing air temperature. TLC, the lower critical temperature, defines the ambient air temperature below which the bird has to expend extra energy to maintain a constant body temperature. To derive species or body mass specific TLC values, an allometric relationship of conductivity for shorebirds has been established by Kersten & Piersma (22, Figure S 11):

$$\text{Conductivity}(\text{W/C}^\circ) = 0.0067 \times BM(kg)^{0.4384} \qquad \text{eqn A15}$$

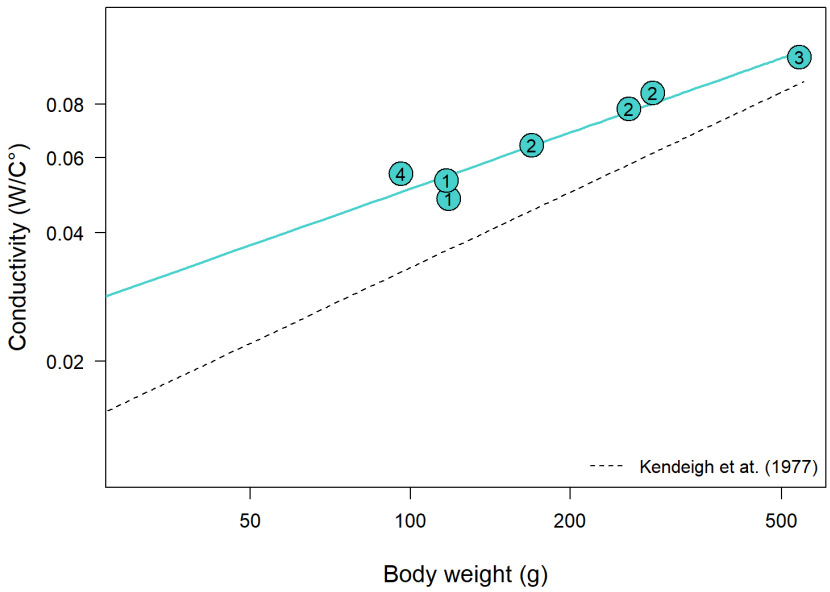

Figure S 11: Allometric relationship of conductance and body weight in shorebirds. Turquoise dots refer to measurements and correlation of conductance in 1. Turnstone, 2. Grey Plover, 3. Oystercatcher, 4. Red Knot (22))

With the body mass specific conductance, we can now derive the lower critical temperature LCT (22):

$$\mathrm{LCT(C°)} = 41° - \frac{BMR_{BM}}{1.2 \times Conductivity_{BM}} \qquad \text{eqn A16}$$

With this, we can calculate species specific and temperature dependent metabolic rates (Figure S 12, left) and transfer the metabolic rates into temperature dependent daily energy expenditure, $DEE(kJ/day) = 2 \times MR_{BM,Temperature} \times 86.4$).

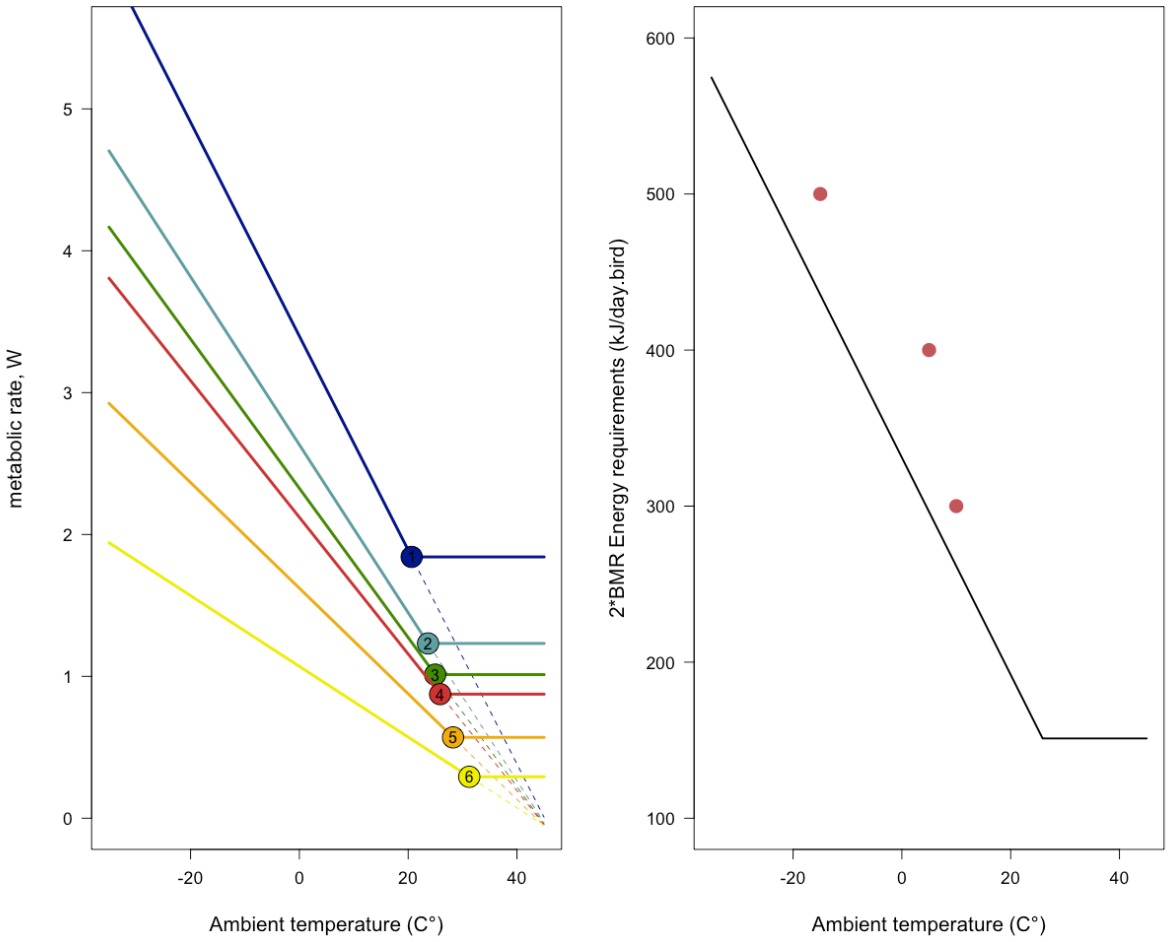

Figure S 12: Metabolic rate in relation to air temperature of six shorebird species (1 Red-necked Stint, 2 Sanderling, 3 Curlew Sandpiper, 4 Red Knot, 5 Great Knot, 6 Bar-tailed Godwit). Dots represent TCL. Right panel shows predicted energy requirement in kJ/day for Red knots (with empirical data from Ens et al. (23)).

Flight capacity

Flight speed differs across species with a slight increase with body mass. Air speed has been observed for several wader species: Bar-tailed Godwits showed a median air speed of 14.4 m/s (± 1.97 SD) and a Dunlin (similar body mass than a Sanderling) had an air speed of 16.1 m/s (± 1.13 SD). Given these relatively small differences in air speed between species with much greater differences in body mass and factors other than body mass (such as wind) likely being more influential, we used a median air speed of 16.7 m/s for all species.
Kvist et al. (24) studied the flight costs of unrestrained Red Knots flying in a wind tunnel, including individuals carrying very high fuel loads. Based on their results, the flight range of

a Knot flying in still air taking off with a body mass of 210 g (max. weight) and arriving with a body mass of 110 g (lean BM) has a flight range of 3420 km. The flight speed of a migrating Red knot is estimated at 60 km/h (16.7 m/s) (25). This means, that a Red Knot flying all day in still air will cover 1440 km per day. However, our empirical tracking data suggest larger flight ranges of up to 4200 km. In addition, geolocator tracking data revealed approximate maximum flight ranges of 5500 km for Great knot and 1800 for Red-necked stints. We used these observations, fitted a linear regression, and extracted the resulting maximum flight ranges for all species.

Table S 2: Species specific parameters derived through allometric scaling.

Species	BM_{min} *[g]*	BM_{max} *[g]*	*g|x|kJ*	FDR_{max} *[x/d]*	*DTR [d]*	*BMR [x/d]*	K_{esm} *[°C]*	*Flight range [km]*
Bar-tailed Godwit	250	534	1|2.84|93.2	5.16	19.66	1.84	20.6	12.650
Great Knot	144	303	1|1.59|52.3	5.99	16.66	1.23	23.6	9.540
Red Knot	105	208	1|1.19|39.2	6.45	15.50	1.01	24.9	8.335
Curlew Sandpiper	55	110	1|0.49|16.1	7.98	12.52	0.56	29.2	5.700
Red-necked Stint	23	45	1|0.13|4.5	10.22	9,78	0.29	31.2	3.800

SI References

1. M. S. Witter, I. C. Cuthill, The ecological costs of avian fat storage. *Philosophical Transactions - Royal Society of London, B* **340**, 73-92 (1993).
2. P. Wiersma, T. Piersma, Effects of Microhabitat, Flocking, Climate and Migratory Goal on Energy Expenditure in the Annual Cycle of Red Knots. *Condor* **96**, 257-279 (1994).
3. M. Klaassen, A. A. Lindstrom, H. Meltofte, T. Piersma, Ornithology. Arctic waders are not capital breeders. *Nature* **413**, 794 (2001).
4. D. Lack, Bird migration and natural selection. *Oikos* **33**, 228–232 (1968).
5. A. I. Houston, J. M. McNamara, J. M. C. Hutchinson, General results concerning the trade-off between gaining energy and avoiding predation. *Philosophical Transactions of the Royal Society B: Biological Sciences* **341**, 375-397 (1993).
6. T. Alerstam, A. Hedenström, The development of bird migration theory. *Journal of Avian Biology* **29**, 343-369 (1998).
7. J. M. McNamara, J. N. Webb, E. J. Collins, T. Székely, A. I. Houston, A General Technique for Computing Evolutionarily Stable Strategies Based on Errors in Decision-making. *Journal of Theoretical Biology* **189**, 211-225 (1997).
8. E. Kalnay *et al.*, The NCEP/NCAR 40-Year Reanalysis Project. *Bulletin of the American Meteorological Society* **77**, 437-471 (1996).
9. NOAA (The NOAA GEO-IDE UAF ERDDAP. (NOAA).
10. C. C. C. S. (C3S), CMIP6 climate projections. Deposited 01.11.2023.
11. N. J. Murray *et al.*, The global distribution and trajectory of tidal flats. *Nature* **565**, 222-225 (2019).
12. N. J. Murray, R. S. Clemens, S. R. Phinn, H. P. Possingham, R. A. Fuller, Tracking the rapid loss of tidal wetlands in the Yellow Sea. *Frontiers in Ecology and the Environment* **12**, 267-272 (2014).
13. C. Giri *et al.*, Status and distribution of mangrove forests of the world using earth observation satellite data. *Global Ecology and Biogeography* **20**, 154-159 (2011).
14. D. A. Robinson, T. W. Estilow, N. C. D. R. Program (2012) NOAA Climate Date Record (CDR) of Northern Hemisphere (NH) Snow Cover Extent (SCE). (NOAA National Centers for Environmental Information).
15. J. del Hoyo, A. Elliot, D. A. Christie, *Handbook of the birds of the world* (Lynx, Barcelona, 2010), vol. 16.
16. U. G. v. Blotzheim, *Handbuch der Vögel Mitteleuropas Band 8 I Teil Charadriiformes 3.Teil* (Akademische Verlagsgesellschaft, Wiesbaden, 1982).
17. A. Lindström, Maximum Fat Deposition Rates in Migrating Birds. *Ornis Scandinavica* **22**, 12-19 (1991).
18. J. K. Kirkwood, A limit to metabolisable energy intake in mammals and birds. *Comparative Biochemistry and Physiology Part A: Physiology* **75**, 1-3 (1983).
19. Y. Aharon-Rotman, K. Gosbell, C. Minton, M. Klaassen, Why fly the extra mile? Latitudinal trend in migratory fuel deposition rate as driver of trans-equatorial long-distance migration. *Ecology and Evolution* **6**, 6616-6624 (2016).

20. M. Klaassen, H. H. Hangelbroek, T. de Boer, B. A. Nolet, Insights from the eco-physiological book of records: Bewick's swans outperform the canonical intake-maximizing vertebrate. *Oikos* **119**, 1156-1160 (2010).
21. J. Aschoff, H. Pohl, Rhythmic variations in energy metabolism. *Fed Proc* **29**, 1541-1552 (1970).
22. M. Kersten, T. Piersma, High Levels of Energy Expenditure in Shorebirds; Metabolic Adaptations to an Energetically Expensive Way of Life. *Ardea* **75**, 175-187 (1987).
23. B. J. Ens, H. Schekkerman, I. Tulp, S. Bauer, M. Klaassen, *Modellling the flyway of arctic breeding shorebirds* (Alterra, Wageningen, 2006).
24. A. Kvist, A. Lindstrom, M. Green, T. Piersma, G. H. Visser, Carrying large fuel loads during sustained bird flight is cheaper than expected. *Nature* **413**, 730-732 (2001).
25. T. Piersma, S. van de Sant, Pattern and predictability of potential wind assistance for waders and geese migrating from West Africa and the Wadden Sea to Siberia. *Ornis svecica* **2**, 55-66 (1992).